Synthesis and optoelectronic properties of the hexa-peri-hexabenzoborazinocoronene

Jacopo Dosso, Jonathan Tasseroul, Francesco Fasano, Davide Marinelli, Nicolas Biot, Andrea Fermi, and Davide Bonifazi*

[*] J. Dosso, F. Fasano, D. Marinelli, N. Biot, Dr. A. Fermi, Prof. Dr. D. Bonifazi
School of Chemistry, Cardiff University, Main Building, Park Place, Cardiff CF10 3AT, United Kingdom; E-mail: bonifazid@cardiff.ac.uk

Dr. J. Tasseroul, Prof. Dr. D. Bonifazi
Department of Chemistry, University of Namur (UNamur), Rue de Bruxelles 61, Namur 5000, Belgium.

[**] D.B. gratefully acknowledges the EU through the ERC Starting Grant "COLORLANDS" project. J.T. thanks the FRS-FNRS for his FRIA doctoral fellowship. The authors also acknowledge the use of the Advanced Computing @Cardiff (ARCCA) at Cardiff University, and associated support services.

Supporting information for this article is available on the WWW under http://www.angewandte.org or from the author. Crystallographic data (excluding structure factors) for the structures reported in this paper have been deposited at the Cambridge Crystallographic Data Centre as supplementary publication no. 1523993 (**1**), 1523994 (**2**), 1523995 (**5**).

Keywords: polycyclic aromatic hydrocarbons, heteroatom doping, boron nitrides, supramolecular chemistry, borazine, hexabenzocoronenes.

Abstract: The first rational synthesis of a BN-doped coronene derivative in which the central benzene ring has been replaced by a borazine core, is described. This includes six C-C ring-closure steps that, through intramolecular Friedel-Crafts-type reactions, allow the stepwise planarization of the hexaarylborazine precursor. All together, UV-vis absorption, emission and electrochemical investigations show that the introduction of the central BN core induces a dramatic widening of the HOMO-LUMO gap and an enhancement of the blue-shifted emissive properties with respect to its all-carbon congener.

Figure to the table of contents

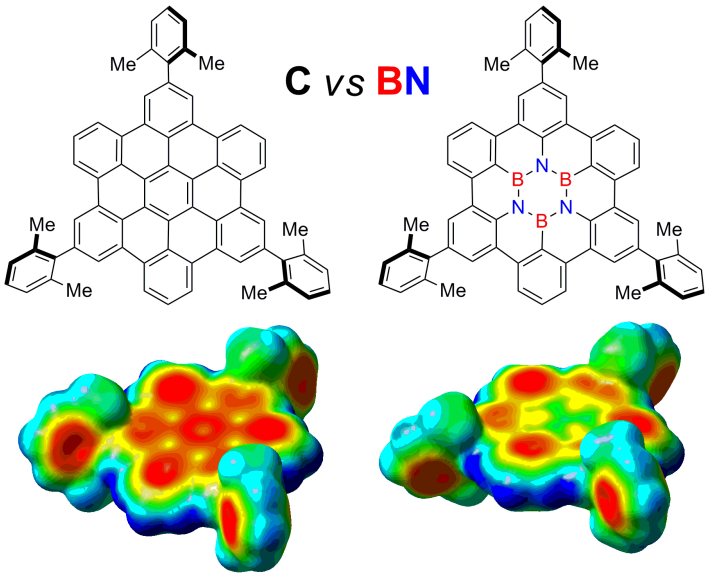

Graphene is one of the leading materials in today's science,[1] but the lack of a bandgap limits its application to replace semiconductors in optoelectronic devices.[2] To overcome this limitation, the replacement of C=C bonds by isostructural and isoelectronic bonds like polar B=N,[3] is emerging as an effective strategy to open a bandgap in monoatomic graphene layers.[4] To the best of our knowledge, only one example of a BN-doped covalent network featuring a regular doping pattern has been described so far through surface-assisted reaction.[5] Otherwise, only sheets containing B, N and C (*h*-BNC) over wide compositional ranges randomly distributed in domains of *h*-BN and graphitic phases have been prepared so far.[6] At the molecular level, notable examples include BN-doped polycyclic aromatic hydrocarbons.[7] Among those, the isolation of the first hexa-peri-hexabenzoborazinocoronene (HBBNC)[8] from pyrolysis of a borazino precursor by Bettinger and co-workers is an important example in view of the creation of hybrid graphenes featuring controlled BN-doping patterns (Figure 1). However, the stunted solubility of this molecule limited in-depth structural and physical studies.

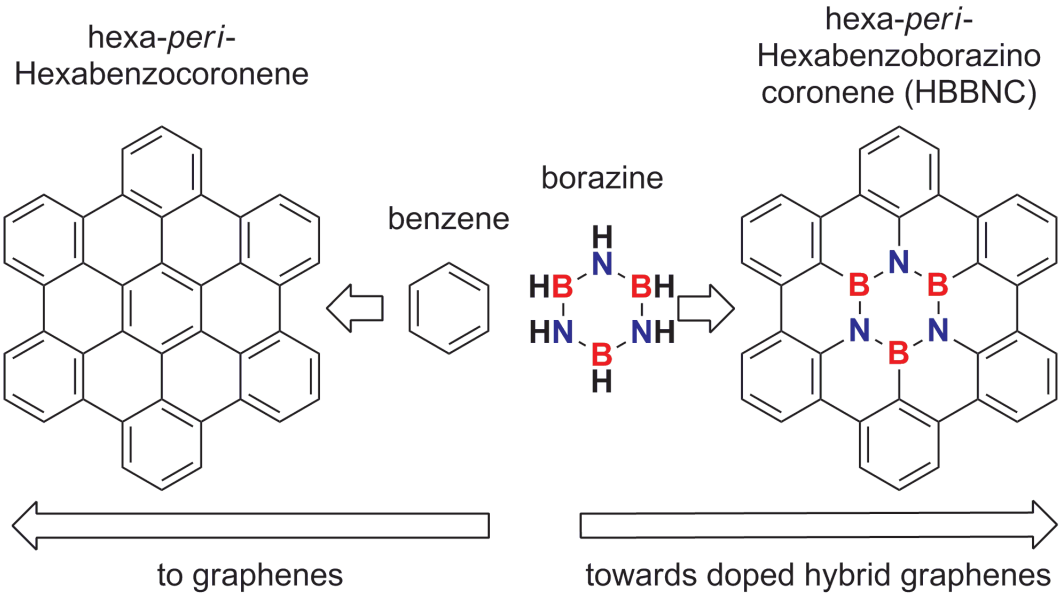

Figure 1. HBC and its borazino-doped analogue HBBNC.

Herein we describe the first rational synthesis of B_3N_3-doped benzocoronene **1** that, being soluble in common organic solvents,

allowed a direct comparison of optoelectronic properties with those of its full-carbon congener. Generally, controlled BN-doping patterns in PAHs are obtained through bottom-up synthesis involving aniline-type precursors[3] that undergo planarization through intramolecular electrophilic aromatic substitution reactions, simultaneously forming C-B and B-N bonds in the presence of BCl_3 and a Lewis acid. At the synthetic planning level, this consideration guided us to contemplate at first a convergent path relegating the formation of the HBBNC core to the last step (Scheme 1, path A). However, the scarce yield for preparing the triamino-spherand precursor forced us to defer this synthetic path and to anticipate the B_3N_3 formation in an earlier step.

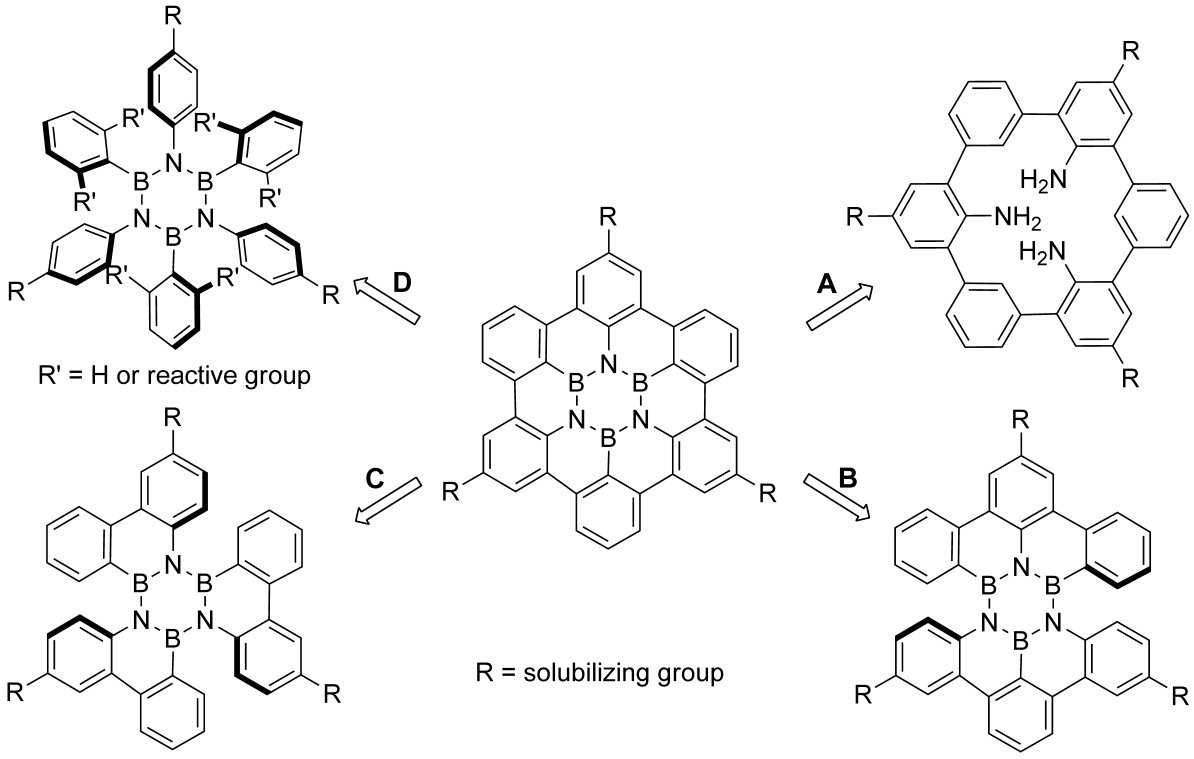

Scheme 1. Retro-synthetic strategies toward HBBC.

This would lead to the HBBNC core through two, three or six ring-closure reactions involving the aryl substituents (Scheme 1, paths B, C and D). As we have predicted a potential instability of the strained borazine precursors[9] of paths B & C, a decision was made to undertake plan D. Commonly, the planarization of covalently-preorganized aryl moieties into PAHs is obtained through Scholl-

type oxidative ring-closure reactions.[2b,10] However, the vulnerability of the borazine ring under oxidative conditions[11,3c] directed us to consider a Friedel-Craft-type substitution as the planarization reaction. This line of thought led us back to hypothetical borazine precursors bearing appropriate leaving groups (L_G) at the *ortho* positions of the B-aryl substituents (path D) that, triggered under given conditions, can yield reactive arylium species. One can hardly fail to notice that the presence of *ortho* L_G additionally exerts protection to the B-atom centers, making the borazine precursor enough stable to be handled. Embracing this synthetic strategy, we prepared a borazine precursor bearing F and peripheral xylyl moieties as LGs and solubilizing groups, respectively.

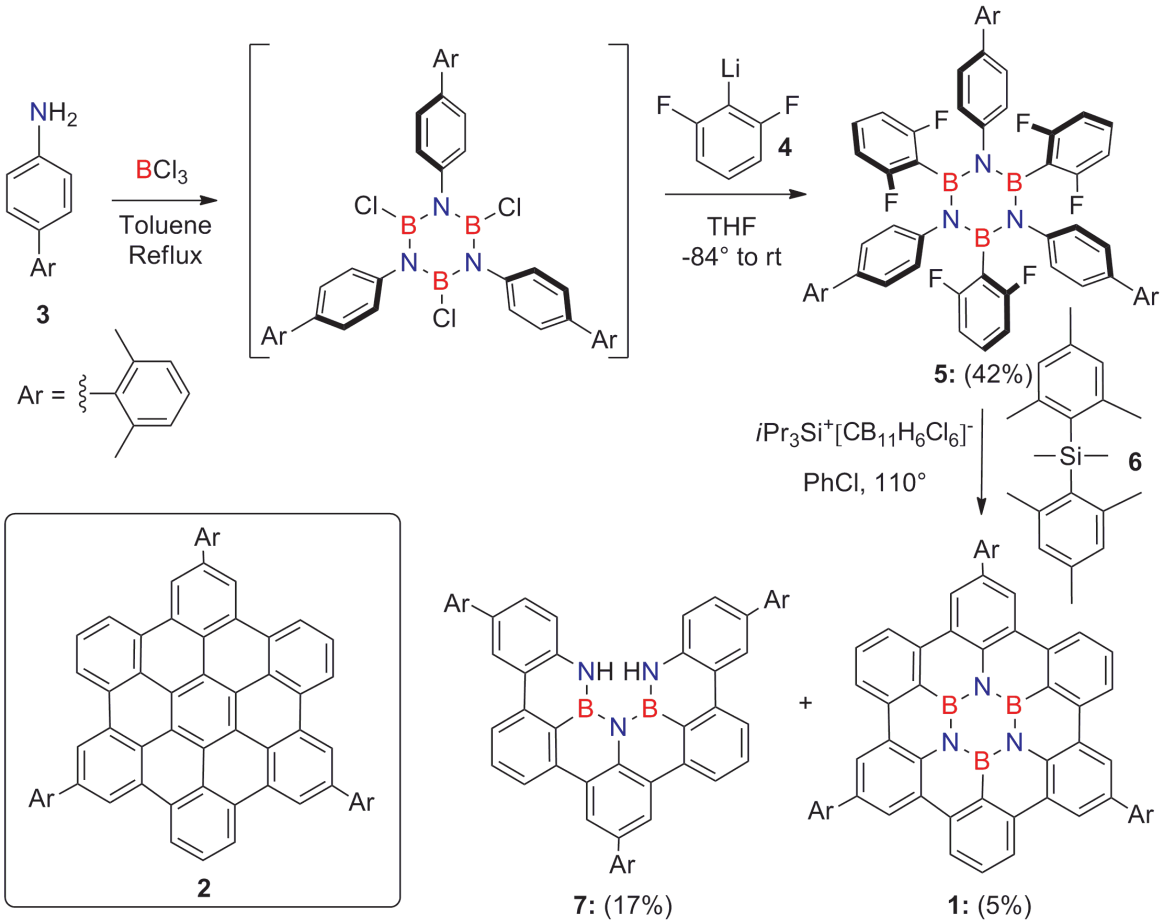

Scheme 2. Synthetic path for preparing xylyl-substituted HBBNC **1**; full-carbon congener **2**.[13]

Following literature protocols,[12] hexafluoro borazine **5** was thus obtained after reaction of 4-xylyl aniline **3** with BCl_3 upon subsequent addition of difluoro ArLi **4** (Scheme 2). A crystal of

borazine **5**, suitable for X-ray diffraction, was obtained by vapor diffusion of MeOH to a CH_2Cl_2 solution of **5** (Figure 2). The quasi-orthogonal arrangement of the aryl moieties forces the F substituents to nest atop the B atoms (B···F = 2.922 Å), negatively shielding the electrophilic center. Capitalizing on the Friedel-Crafts ring-closure reaction of fluoroarenes developed by *Siegel* and co-workers,[14] borazine **5** could be planarized into HBBNC **1** (5%, 61% per C-C bond formation) in the presence of $[iPr_3Si{\cdots}CB_{11}H_6Cl_6]$ and Me_2SiMes_2 at 110 °C in PhCl operating in a *Schlenk* line. Together with HBBNC **1**, partially fused BN-derivative **7** was obtained as major product (17% yield), suggesting that the ring closure proceeds stepwise with the last aryl fusion likely being the rate-determining step. All-carbon congener HBC **2** (Scheme 2) was also prepared for comparison purposes (Scheme S1, SI).[13]

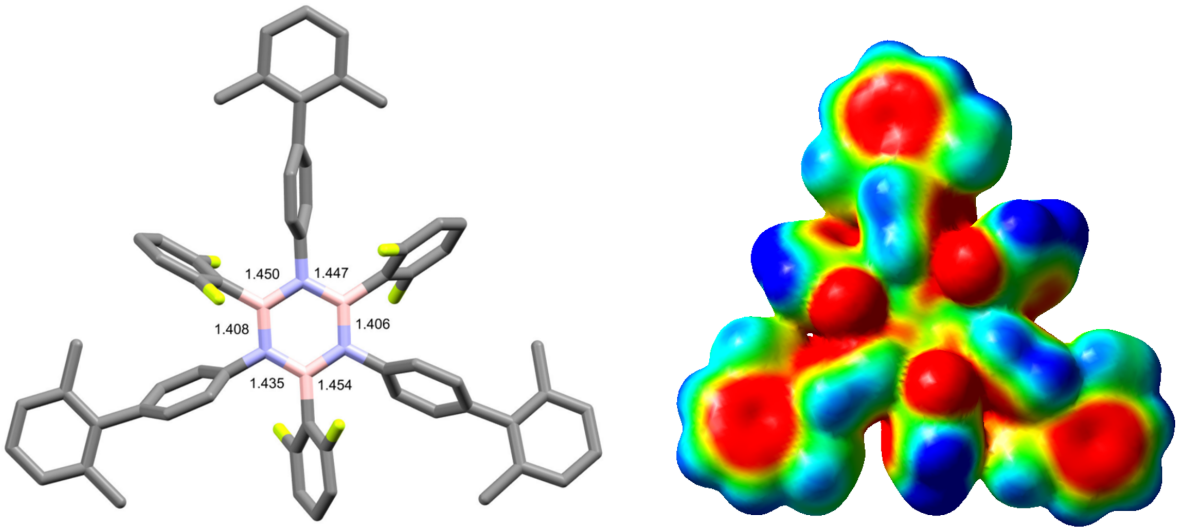

Figure 2. X-ray structure and ESP mapped on the vdW surface up to an electron density of 0.001 electron.bohr^{-3} for **5**. Atom colors: pink B, blue N, green F, gray C; space group: $P2_1/c$. B-N distances in Å are shown.

Molecule **1** was characterized using NMR, UV/Vis, IR spectroscopies and HR-MALDI spectrometry. At first, HBBNC **1** was unambiguously identified by HR-MALDI through the detection of the peak corresponding to the molecular ion at m/z 837.3652 ($C_{60}H_{42}B_3N_3^+$, calc.: 837.3658). Solution ^{1}H-NMR spectra further confirmed the structure of HBBNC **1** (Figure 3B). Specifically, coupled H_a and H_b protons appear as triplet (8.05 ppm) and doublet (8.55 ppm), respectively, whereas one singlet (8.58 ppm) is observed for H_c

proton. An analogous resonance pattern (Figure 3A) is also observed for reference **2**. Notably, the presence of the inner B_3N_3 cycle in **1** induces a high-field shift of the proton resonances with respect to those of **2**, suggesting a significant decrease of the magnetic anisotropic properties of the B_3N_3-doped derivative. Analogously, a remarkable high-field shift was also observed for the boron resonance (at 30.59 ppm) in the ^{11}B-NMR spectrum (Figure S24) of **1** when compared to that of precursor **5** (at 34.9 ppm).

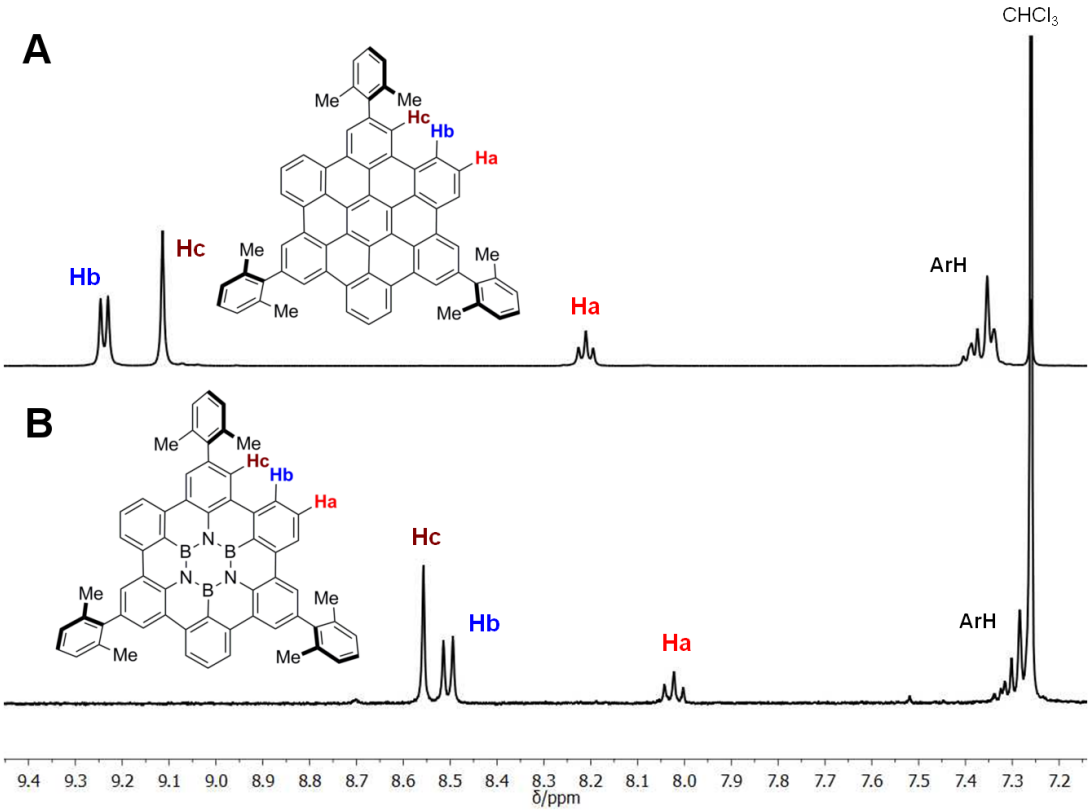

Figure 3. Exerts of the ^{1}H-NMR spectra (400 MHz, $CDCl_3$) in the aromatic region for HBBNC **1** (bottom) and HBC **2** (above).

To further corroborate the chemical structure of **1**, crystals suitable for X-ray diffraction analysis were obtained by vapour diffusion of *i*PrOH to a C_6H_6 solution of **1** (Figure 4A). The X-ray analysis confirms the nearly flat shape of the BNC framework, displaying a similar structure to that of all-carbon congener **1**, with shorter B-N lengths (1.433 – 1.442 Å, Figure 4A) than those measured in hexagonal boron nitride (*h*-BN, 1.446 Å). To appraise the effect of the BN doping on the aromatic π-surface, we further determined the charge distribution of the crystal structure of **1**

in the form of ESP (Figure 4B) calculated with Gaussian 09 at B3LYP/6-31G(d,p) level of theory (SI).

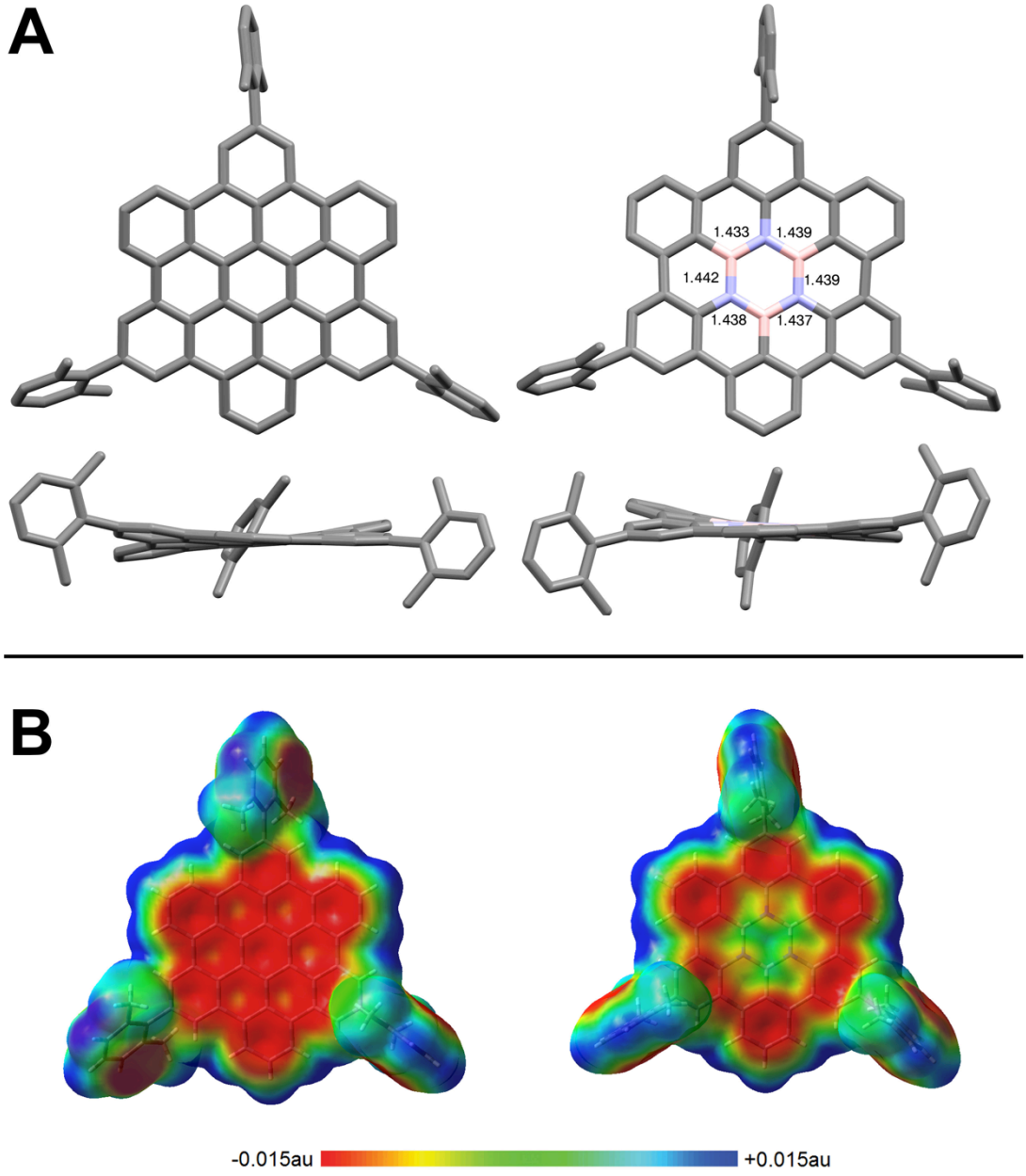

Figure 4. A: Horizontal (top) and side (bottom) view of the X-ray crystal structures of HBBNC (with the B-N distances in Å) **1** (right) and HBC **2** (left). Atom colors: pink B, blue N, gray C; space groups: I2/a and P-1, respectively. **B:** ESP mapped on the vdW surface up to an electron density of 0.001 electron.bohr^{-3}.

As expected, the π-surface of **2** is negatively charged showing the presence of a homogenous π-cloud above and below the HBC skeleton. On the other hand, **1** displays a great charge polarization of the π-surface, with the N and B atoms negatively and positively charged,

respectively, and the outer hexaphenylene rim negatively charged. These results are consistent with the expected ambipolar character of the molecule.[15] UV-vis absorption and emission properties in CH_2Cl_2 of molecules **1** and **2** are displayed in Figure 5 and Table 1. The lowest-energy electronic transition of **1** appears in the near-UV (375 nm) at significantly higher energy with respect to that of **2** (446 nm). In line with theoretical predictions,[4a-b,11] this finding suggests that the B_3N_3-doping widens the molecular optical bandgap (ΔE_{opt} = 0.53 eV). In addition, the absorption bands of **1** show noticeable vibrational substructures evidencing a high degree of rigidity of the molecular skeleton.[16]

Table 1. Photophysical data for **1** and **2** in solution and at the solid state.

	Absorption	**Emission**					
Molecule	λ (nm) (ε, M^{-1} cm^{-1})[a]	$\lambda_{max,fl}$ (nm)	$E_{opt,fl}$ (eV)[b]	τ_{fl} (ns)	Φ_{fl}[c]	$\lambda_{max,PH}$ (nm)[d]	τ_{ph} (s)[d]
2 (CH_2Cl_2)	446 (1000) 388 (53800) 358 (159100)	485[a]	2.76	16.4[a] 27.9[f]	0.03[a] 0.05[f]	570	0.8
2 (solid)	-	487	-	3.7(64%)[e] 12.1(36%)[e]	-	-	-
1 (CH_2Cl_2)	375 (24000) 314 (31200)	404[a]	3.29	8.2 [a] 10.9[f]	0.43[a] 0.77[f]	492	4.0
1 (solid)	-	426	-	1.5(43%)[e] 8.0(57%)[e]	-	-	-

[a]Recorded in air-equilibrated CH_2Cl_2 at rt [b]Calculated from the higher-energy maxima of the emission spectra in air-equilibrated CH_2Cl_2 at rt (E_{opt} = 1240/λ_{fl}). [c]Quinine sulfate in 0.5 M H_2SO_4 was used as the standard (Φ_{QS} = 0.546). [d]Recorded in a 1:1 CH_2Cl_2:CH_3OH v/v rigid matrixes at 77 K (Figure S31). [e]Fitting of the emission decays are biexponential. [f]Calculated for O_2-free solutions.

Consistently, the emission spectra (Figure 5) in solution at rt reflect the same trend, with the intense emission peak of **1** (λ_{max} = 404 nm, Φ_{fl} = 0.43) significantly blue-shifted with respect to that of **2** (λ_{max} = 485 nm). Notably, the Φ_{fl} value significantly increases to 0.77 in O_2-free solutions. Phosphorescence spectra at low temperature (Figure 5) showed long-lasting emission profiles (τ_{Phos} = 4 s) with **1** providing the highest-energy triplet emission ($\lambda_{max,Phos}$ = 492 and 570 nm for **1** and **2**, respectively).[17] Furthermore, **1**

displays appreciable solid-state fluorescence emission in the violet-blue region (λ_{max} = 426 nm *vs* λ_{max} = 487 nm for **2**) at rt (Figure S32).

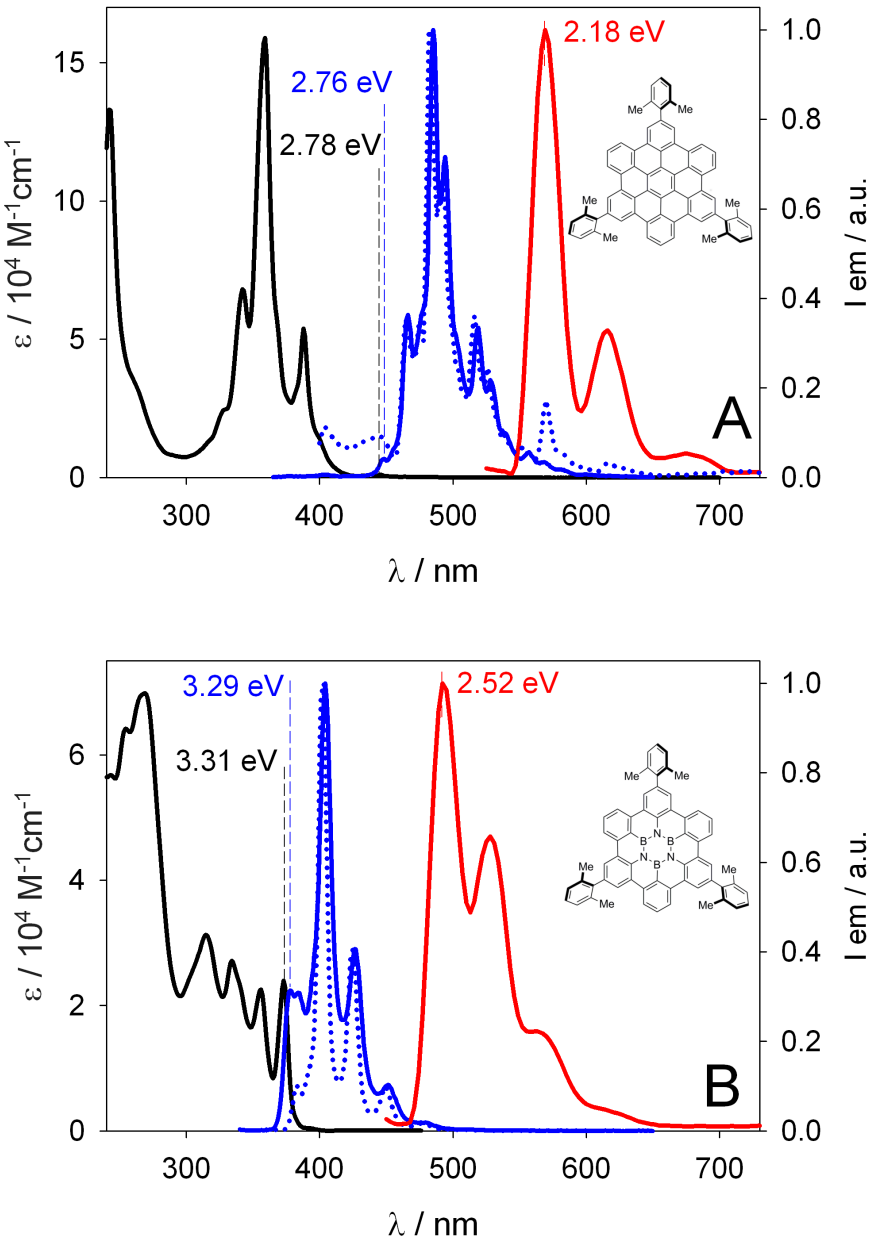

Figure 5. Absorption (black) and normalized fluorescence (blue) spectra of **1** (**B**, λ_{ex} = 315 nm) and **2** (**A**, λ_{ex} = 355 nm) in air equilibrated CH_2Cl_2 at rt; fluorescence (blue dotted) and phosphorescence (red) spectra at 77 K in a CH_2Cl_2:CH_3OH (1:1, v/v) rigid matrix.

Cyclic voltammetry (CV) measurements showed a quasi-reversible first oxidation wave at approximately 1.46 V *vs*. SCE in CH_2Cl_2 for HBBNC **1** (Figures 6 and S34), which is considerably higher in

energy with respect to that of its carbon congener ($E_{1/2ox}$= 1.27 V vs. SCE).[18] On the other hand, no relevant reduction waves were detected at any scan rates under the same experimental conditions for both molecules. Taken together, these data allowed us to estimate the energies of the HOMO and LUMO orbitals, resulting to be -5.80 (HOMO) and -2.51 eV (LUMO) for **1** and -5.61 (HOMO) and -2.85 eV (LUMO) for **2** (Figure 6 and Table S4). To shed further light on the structure-property relation, we calculated the HOMO and LUMO orbitals for **1** and **2** (Figure 6 and S35). As observed by others,[4a-b,11] it transpires that both orbitals are homogenously distributed on the π-surface of **2**, whereas the LUMO for **1** is only located on the hexaphenylene rim. This suggests that the one-e$^-$ reduction of **1** is likely to be confined on the hexaphenylene periphery excluding the B_3N_3 ring, whereas that of **2** is localized on the entire carbon π-surface.

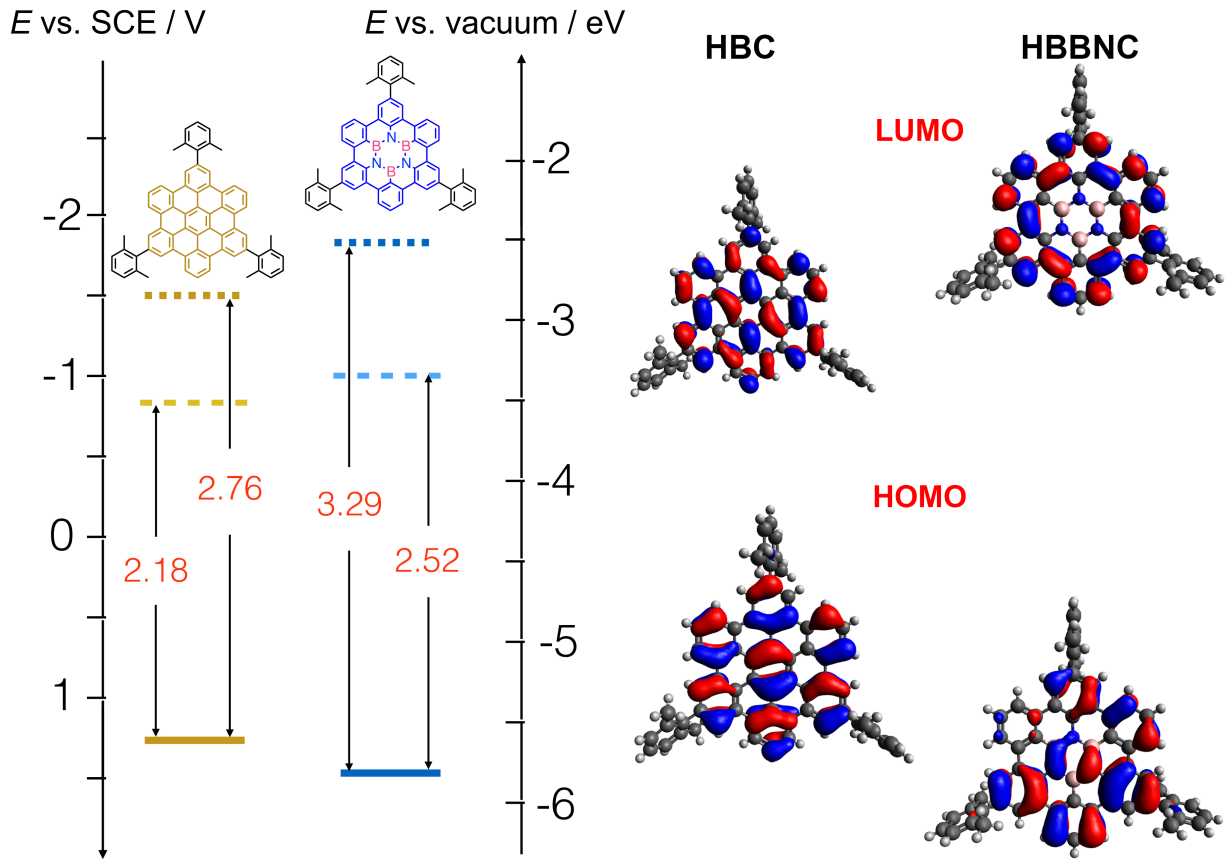

Figure 6. Left. Frontier orbital energies estimated from the CV and photophysical data for **1** and **2**. Reduction potentials of the triplet excited states are evidenced by the narrower optical energy gaps (E^T* = $E^{1/2}{}_{ox}$-$E_{opt}{}^T$).

Fc^+/Fc = 0.46 V vs. SCE; -4.8 eV *vs* vacuum. **Right.** HOMO and LUMO profiles for **1** and **2** at B3LYP/6-31G(d,p) level of theory (GAUSSIAN09).

In conclusion, in this paper we have described the first synthetic methodology to prepare a soluble HBBNC molecule following a planarization strategy based on a Friedel-Crafts reaction. This involves the simultaneous formation of six C-C bonds starting from a hexafluoro borazine precursor. First X-ray diffraction confirmed the presence of the inner B_3N_3 cycle, with short B-N bond lengths. The remarkable UV absorption, strong blue-violet singlet emission, and green phosphorescence of this class of hybrid B_3N_3-doped molecules are in line with the theoretical predictions. Given the importance and ubiquity of graphene in scientific research, the development of novel synthetic strategies leading to hybrid graphene derivatives featuring precise doping patterns will undoubtedly lead to new discoveries and applications in materials science. In this respect, the synthesis and photophysical study of this long-awaited compound marks an important milestone toward the understanding of the optoelectronic properties of doped molecular graphenes.

References

[1] a) S. Park, R. S. Ruoff, *Nat. Nanotechnol.* **2009**, *4*, 217–224; b) F. Schwierz, *Nat. Nanotechnol.* **2010**, *5*, 487–496.

[2] a) J. Wu, W. Pisula, K. Müllen, *Chem. Rev.* **2007**, *107*, 718–747; b) A. Narita, X. Wang, X. Feng, K. Müllen, *Chem. Soc. Rev.* **2015**, *44*, 6616–6643.

[3] a) Z. Liu, T. B. Marder, *Angew. Chem. Int. Ed.* **2008**, *47*, 242–244; b) X. Wang, J. Wang, J. Pei, *Chem. Eur. J.* **2015**, *21*, 3528–3539; c) D. Bonifazi, F. Fasano, M. M. Lorenzo-Garcia, D. Marinelli, H. Oubaha, J. Tasseroul, *Chem. Commun.* **2015**, *51*, 15222–15236; d) H. Helten, *Chem. Eur. J.* **2016**, *22*, 12972–12982;

[4] a) W. Xie, T. Yanase, T. Nagahama, T. Shimada, *C* **2016**, *2*, 1–9; b) N. Otero, K. E. El-kelany, C. Pouchan, M. Rérat, P. Karamanis, *Phys. Chem. Chem. Phys.* **2016**, *18*, 25315–25328; c) N. Otero, P. Karamanis, K. E. El-Kelany, M. Rérat, L. Maschio,

B. Civalleri, B. Kirtman, *J. Phys. Chem. C,* **2017**, *121*, 709–722.

[5] C. Sánchez-Sánchez, S. Brüller, H. Sachdev, K. Müllen, M. Krieg, H. F. Bettinger, A. Nicolaï, V. Meunier, L. Talirz, R. Fasel, P. Ruffieux, *ACS Nano*, **2015**, *9*, 9228–9235;

[6] a) L. Ci, L. Song, C. Jin, D. Jariwala, D. Wu, Y. Li, A. Srivastava, *Nat. Mater.* **2010**, *9*, 430–435; b) C. Huang, C. Chen, M. Zhang, L. Lin, X. Ye, S. Lin, M. Antonietti, X. Wang, *Nat. Commun.* **2015**, *6*, 7698-7704.

[7] Selected examples: a) G. C. Culling, M. J. S. Dewar, P. A. Marr, *J. Am. Chem. Soc.* **1964**, *86*, 1125-1127; b) M. J. D. Bosdet, C. A. Jaska, W. E. Piers, T. S. Sorensen, *Org. Lett.* **2007**, *9*, 1395–1398; c) M. J. D. Bosdet, W. E. Piers, T. S. Sorensen, M. Parvez, *Angew. Chem. Int. Ed.* **2007**, *46*, 4940–4943; d) A. J. V. Marwitz, M. H. Matus, L. N. Zakharov, D. A. Dixon, S.-Y. Liu, *Angew. Chem. Int. Ed.* **2009**, *48*, 973-977; e) T. Hakateyama, S. Hashimoto, S. Seki, M. Nakamura, *J. Am. Chem. Soc.* **2011**, *133*, 18614–18617; f) J. S. A. Ishibashi, J. L. Marshall, A. Mazie, G. J. Lovinger, B. Li, L. N. Zakharov, A. Dargelos, A. Gracia, A. Chrostowska, S. Liu, *J. Am. Chem. Soc.* **2014**, *136*, 15414–15421; g) G. A. Molander, S. R. Wisniewski, *J. Org. Chem.* **2014**, *79*, 6663–6678; h) H. Braunschweig, M. A. Celik, F. Hupp, I. Krummenacher, L. Mailänder, *Angew. Chem. Int. Ed.* **2015**, *54*, 6347-6351; i) X. Wang, F. Zhang, K. S. Schellhammer, P. Machata, F. Ortmann, G. Cuniberti, Y. Fu, J. Hunger, R. Tang, A. A. Popov, R. Berger, K. Müllen, X. Feng, *J. Am. Chem. Soc.* **2016**, *138*, 11606-11615; j) M. Numano, N. Nagami, S. Nakatsuka, T. Katayama, K. Nakajima, S. Tatsumi, N. Yasuda, T. Hatakeyama, *Chem. Eur. J.* **2016**, *22*, 11574–11577.

[8] a) M. Krieg, F. Reicherter, P. Haiss, M. Ströbele, K. Eichele, J. Treanor, R. Schaub, H. F. Bettinger, *Angew. Chem. Int. Ed.* **2015**, *54*, 8284–8286; b) F. Ciccullo, A. Calzolari, I. Píš, S. A. Savu, M. Krieg, H. F. Bettinger, E. Magnano, T. Chassé, and M. B. Casu, *J. Phys. Chem. C*, **2016**, 120, 17645–17651.

[9] S. Biswas, M. Müller, C. Tönshoff, K. Eichele, C. Maichle-mössmer, A. Ruff, B. Speiser, H. F. Bettinger, *Eur. J. Org. Chem.* **2012**, 4634–4639.

[10] M. D. Watson, A. Fechtenkötter, K. Müllen, *Chem. Rev.* **2001**, *101*, 1267–1300.

[11] C. Tönshoff, M. Müller, T. Kar, F. Latteyer, T. Chassé, K. Eichele, H. F. Bettinger, *ChemPhysChem* **2012**, *13*, 1173–1181.

[12] a) S. J. Groszos, S. F. Stafiej, *J. Am. Chem. Soc.* **1958**, *80*, 1357–1360; b) A. Wakamiya, T. Ide, S. Yamaguchi, *J. Am. Chem. Soc.* **2005**, *127*, 14859–14866; c) S. Kervyn, O. Fenwick, F. Di Stasio, Y. Sig Shin, J. Wouters, G. Accorsi, S. Osella, D. Beljonne, D. Bonifazi, *Chem. Eur. J.* **2013**, *19*, 7771–7779; d) S. Kervyn, N. Kalashnyk, M. Riello, B. Moreton, J. Tasseroul, J. Wouters, T. S. Jones, A. De Vita, G. Costantini, D. Bonifazi, *Angew. Chem. Int. Ed.* **2013**, *52*, 7410–7414.

[13] R. Yamaguchi, S. Hiroto, H. Shinokubo, *Org. Lett.* **2012**, *14*, 2472–2475.

[14] O. Allemann, S. Duttwyler, P. Romanato, K. K. Baldridge, J. S. Siegel, *Science* **2011**, *332*, 574–577.

[15] E. Vessally, S. Soleimani-amiri, A. Hosseinian, L. Edjlali, A. Bekhradnia, *Appl. Surf. Sci.* **2017**, *396*, 740–745.

[16] X. Wang, F. Zhuang, R. Wang, X. Wang, X. Cao, J. Wang, J. Pei, *J. Am. Chem. Soc.* **2014**, *136*, 3764–3767.

[17] S. Hashimoto, T. Ikuta, K. Shiren, S. Nakatsuka, J. Ni, M. Nakamura, T. Hatakeyama, *Chem. Mater.* **2014**, *26*, 6265–6271.

[18] a) A. Stabel, P. Herwig, K. Müllen, J. P. Rabe, *Angew. Chem. Int. Ed. Engl.* **1995**, *34*, 1609–1611; b) R. Rathore, C. L. Burns, *J. Org. Chem.* **2003**, *68*, 4071–4074.